Astronomy & Astrophysics manuscript no. output
December 21, 2025

The Impact of Star Formation Histories on the Inner Dark Matter Density Slopes of Galaxies

J. Sarrato-Alós[1,2], J. Bullock[3], A. Di Cintio[2,1], C. Brook[2,1], F. Valenciano[1,2] & A. V. Macciò[4,5]

[1] Instituto de Astrofísica de Canarias (IAC), Calle Via Láctea s/n, E-38205 La Laguna, Tenerife, Spain
e-mail: jorge.sarrato@iac.es
[2] Universidad de La Laguna, Avda. Astrofísico Fco. Sánchez s/n, E-38206 La Laguna, Tenerife, Spain
[3] Department of Physics & Astronomy, University of Southern California, Los Angeles, CA 90089, USA
[4] New York University Abu Dhabi, PO Box 129188, Abu Dhabi, United Arab Emirates
[5] Center for Astrophysics and Space Science, New York University Abu Dhabi, Abu Dhabi, PO Box 129188, Abu Dhabi, UAE

Received x xx, xxxx; accepted x xx, xxxx

ABSTRACT

Aims. We aim to investigate the connection between star formation histories (SFHs) and the inner dark matter density profiles of simulated galaxies. In particular, we test whether the burstiness and temporal distribution of star formation influence the formation of cored versus cuspy dark matter profiles.

Methods. We homogeneously analysed simulated galaxies from the NIHAO and FIRE-2 projects. For each galaxy, we derived dark matter density profiles and measured the logarithmic slope in the inner region of the dark matter halo (1–2% of R_{vir}). To characterise star formation burstiness, we introduced a criterion based on comparing the star formation rate (SFR) averaged over two distinct timescales. We further quantified the duration of SFHs by computing $M_{\star,\rm post}$ / $M_{\star,\rm pre}$, the ratio of stellar mass formed after versus before the epoch of reionisation at redshift z ∼ 6.5.

Results. Homogeneous analysis reveals that inner slope versus stellar-to-halo mass ratio trends for NIHAO and FIRE-2 galaxies are in much better agreement than reported in previous works. The burstiness and duration of the SFH explain the scatter in the inner slope versus stellar-to-halo mass ratio relation, revealing that galaxies with over average burstiness and more extended SFHs are more efficient at developing cored dark matter profiles. In contrast, galaxies with smoother SFHs and earlier stellar mass assembly tend to maintain cuspier dark matter profiles. We present an analytic expression that improves predictions for the inner slope using the parameter $M_{\star,\rm post}$ / $M_{\star,\rm pre}$, which reduces the mean squared error in both simulation suites relative to previous formulations based solely on the stellar-to-halo mass ratio.

Key words. Dark matter profiles

1. Introduction

Understanding how baryonic processes influence the distribution of dark matter in galaxies is a key objective in the study of galaxy formation and evolution. One of the most studied topics in this area is the discrepancy between the central dark matter profiles predicted by simulations and those inferred from observations of dwarf and low surface brightness galaxies. While cold dark matter only simulations robustly predict cuspy inner profiles (Navarro et al. 1997), observational studies often find shallower, core-like distributions (de Blok et al. 2001; Oh et al. 2011). This "core-cusp" tension has motivated investigation into the potential for baryonic physics (particularly stellar feedback) to modify the dark matter structure found in cold dark matter only simulations, especially in the central regions of galaxies.

An extensive number of theoretical and numerical works have demonstrated that star formation and feedback processes can significantly impact the inner slope of dark matter halos. In particular, the total amount of energy injected by stellar feedback, relative to the total halo mass of the galaxy, plays a critical role in driving dark matter core formation. This property is closely correlated with the stellar-to-halo mass ratio (Peñarrubia et al. 2012; Pontzen & Governato 2012; Brook & Di Cintio 2015). Simulations show that repeated gas outflows associated with star formation can generate potential fluctuations that dynamically heat the dark matter, pushing it outward and flattening the central cusp (Di Cintio et al. 2014a,b; Tollet et al. 2016; Lazar et al. 2020). In particular, Di Cintio et al. (2014b) fitted the relationship between the dark matter profile inner slope and the stellar-to-halo mass ratio using Eq. 1, whilst Tollet et al. (2016) and Lazar et al. (2020) used the more complex Eq. 2, with $x = M_\star/M_{\rm halo}$ in both cases. It is worth noting that different studies adopt different halo mass definitions: some compute the halo mass $M_{\rm halo}$ using an overdensity of 200 times the critical density of the universe (M_{200c}), whereas others use the virial overdensity ($M_{\rm vir}$). Equally, $R_{\rm halo}$ is defined as the radius that encloses a total mass of $M_{\rm halo}$ according to the adopted overdensity. These studies have revealed that core formation is most efficient at intermediate stellar-to-halo mass ratios ($M_\star/M_{\rm halo}$ ∼ 0.005-0.007), providing a useful first order predictor of halo structure.

$$\left.\frac{d\rho}{d\log_{10} r}\right|_{r=0.015R_{\rm halo}}(x) = n - \log_{10}\left[\left(\frac{x}{x_0}\right)^{-\beta} + \left(\frac{x}{x_0}\right)^{\gamma}\right] \quad (1)$$

$$\left.\frac{d\rho}{d\log_{10} r}\right|_{r=0.015R_{\rm halo}}(x) = n - \log_{10}\left[n_1\left(1 + \frac{x}{x_1}\right)^{-\beta} + \left(\frac{x}{x_0}\right)^{\gamma}\right] \quad (2)$$

However, while these results emphasise the importance of integrated stellar feedback over cosmic time, the detailed temporal structure of star formation (the extent to which it is bursty or continuous, or how long the galaxy takes to form its stars) may further modulate the effectiveness of this process. Specifically, it has been proposed that bursty star formation, which drives stronger and more abrupt changes in the gravitational potential, may be more effective at reshaping dark matter distributions than smoother, extended star formation histories with similar total stellar mass (Navarro et al. 1996; Read & Gilmore 2005; Pontzen & Governato 2014). Di Cintio et al. (2017) demonstrated that both the burstiness and overall duration of star formation are key drivers of the structural differences between diffuse and compact galaxies. Systems that experience extended, highly bursty SFHs tend to develop more extended dark matter cores, whereas those with shorter, less bursty SFHs exhibit cuspier central dark-matter profiles and smaller effective radii (see their Fig. 4). This motivates the need to quantify burstiness as a distinct parameter, beyond stellar-to-halo mass ratio, in understanding dark matter core formation.

Apart from burstiness, Muni et al. (2024) highlighted the importance of the duration of the SFH on the process of core formation. Specifically, they found the ratio of stellar mass that formed after and before the re-ionisation epoch shows better correlation with the inner dark matter density of galaxies than the stellar-to-halo mass ratio in the EDGE simulations (Agertz et al. 2019; Rey et al. 2025).

Observational and theoretical efforts have begun to characterise bursty star formation in low mass galaxies (Weisz et al. 2012; Emami et al. 2019), and cosmological simulations increasingly resolve these time variable feedback processes. However, the relationship between star formation burstiness and dark matter structure has yet to be systematically quantified. In particular, it remains unclear whether galaxies with similar star-to-halo mass ratios but different star formation histories exhibit systematically different inner density profiles, and whether burstiness can account for the scatter in the observed relation between the $M_\star/M_{\rm halo}$ ratio and the inner slope.

In this paper, we address this gap by homogeneously analysing two suites of simulated galaxies to quantify the burstiness of their SFHs and measure the corresponding slopes of their dark matter density profiles. We show that galaxies with similar stellar mass but differing degrees of burstiness can present remarkably different inner dark matter structures, with more bursty galaxies tending to produce cored profiles more often. Our results suggest that burstiness introduces an important second order effect that can help explain the diversity in inner halo slopes. Additionally, we find the total duration of star formation after an early time threshold (close to the re-ionisation epoch) has a similar effect to that of burstiness on the inner slope of the dark matter profile. By explicitly linking time resolved star formation behaviour to dark matter core formation, this work offers new insight into the role of baryonic feedback in shaping galaxy structure.

The paper is organised as follows. Section 2 introduces the two suites of simulated galaxies that form the basis of our analysis. In Section 3, we present the main results from the homogeneous analysis of both suites. This section is structured to first address the relationship between the burstiness metric and the inner dark matter profile slopes (Section 3.1). We then investigate the correlation between the total duration of the SFH and the inner dark matter slopes in Section 3.2. Section 3.3 reports an improved fitting equation for the inner slope that combines the effects of the stellar-to-halo mass ratio and the SFH duration. Finally, our conclusions are summarised in Section 4.

2. Simulations

2.1. The NIHAO project

The NIHAO project (Numerical Investigations of Hundred Astrophysical Objects) is a suite of high resolution cosmological zoom-in hydrodynamical simulations based on GASOLINE2 code (Wadsley et al. 2017) and first presented in Wang et al. (2015). The NIHAO project adopts Planck cosmology (Planck Collaboration et al. 2014), using the following parameters: H_0 = 100h km s^{-1} Mpc^{-1} with h = 0.671, $\Omega_{\rm m}$ = 0.3175, Ω_Λ = 0.6824, $\Omega_{\rm b}$ = 0.049, and σ_8 = 0.8344.

NIHAO simulations include all fundamental process involved in galaxy formation. More precisely the implementation of star formation and stellar feedback mechanisms follows the model established in the Making Galaxies In a Cosmological Context (MaGICC; Stinson et al. 2013) simulations. This particular framework has proved success in reproducing a broad range of observed galaxy scaling relations (Brook et al. 2012; Macciò et al. 2012). Star formation is allowed in dense gas that exceeds a density threshold number, set at $n_{\rm th}$ = 10.3 cm^{-3}, using an initial mass function from Chabrier (2003). Feedback includes early energy injection from massive stars and the contribution of supernovae, where the latter is modelled using a blast-wave approach (Stinson et al. 2006).

Gas evolution includes metal-line cooling, photoionisation, and ultraviolet heating, based on the prescriptions detailed by Shen et al. (2010). Specifically, the ultraviolet background is implemented via the Haardt & Madau (2012) model, which leads to the complete ionisation of hydrogen in the intergalactic medium by z ~ 6.7.

The mass and spatial resolution of the simulations allow the inner structure of galaxies to be resolved down to below 1% of the virial radius (e.g. Tollet et al. 2016). Half-light radii are well captured, with spatial resolutions ranging from about 100 pc in low-mass systems to 800 pc in the most massive galaxies.

We used Amiga Halo Finder (AHF Knollmann & Knebe 2009) and selected the main isolated halo from each zoom-in simulation as long as it contained at least one hundred star particles, resulting in a sample of 93 galaxies.

2.2. The FIRE project

The FIRE project comprises several sets of cosmological zoom-in simulations generated with the GIZMO (Hopkins 2015) code, using slightly different cosmological parameters depending on the run. Some follow the Planck cosmology (Planck Collaboration et al. 2014), while others adopt parameters from the Assembling Galaxies Of Resolved Anatomy (AGORA; Kim et al. 2014) project: H_0 = 100h km s^{-1} Mpc^{-1} with h = 0.702, $\Omega_{\rm m}$ = 0.272, Ω_Λ = 0.728, $\Omega_{\rm b}$ = 0.0455, and σ_8 = 0.807.

Specifically, we use the FIRE-2 simulations, which include a detailed model of galaxy formation physics. These include feedback from stars and supermassive black holes, magnetic fields, cosmic rays, and radiation processes such as photoheating and photoionisation. Reionisation is treated via the uniform ultraviolet background of Faucher-Giguère et al. (2009), leading to a fully ionised hydrogen intergalactic medium by z ~ 6. These simulations reach high spatial resolution, with gravitational softening lengths on the order of 10 pc.

The FIRE-2 simulations have been shown to reproduce a broad range of observed galaxy properties. As demonstrated in Hopkins et al. (2018), these include realistic star formation histories, gas distributions, metallicity profiles, morphologies, and rotation curves, as well as stellar mass scaling relations.

We use the FIRE-2 cosmological zoom-in simulations presented in Hopkins et al. (2018) and in Graus et al. (2019). Haloes were again identified using AHF. Exploiting the higher resolution of the FIRE-2 simulations and aiming to improve the statistical robustness of our analysis, we did not restrict our selection to the primary halo in each simulation. Instead, for each simulation, we considered the ten haloes containing the largest number of particles. From these, we kept only those composed of at least 99% high-resolution particles and containing a minimum of a hundred star particles. Applying these criteria results in a sample of 109 isolated galaxies.

3. Results

We defined the virial radius, $R_{\rm vir}$, as the radius enclosing a mean density equal to $\Delta_{\rm vir}$ times the critical density of the universe, $\rho_{\rm crit} = \frac{3H^2}{8\pi G}$, where H is the Hubble parameter and G is the gravitational constant. The value of $\Delta_{\rm vir}$ was calculated using the redshift-dependent prescription from Bryan & Norman (1998), evaluated at $z = 0$. The virial mass was then obtained by summing the masses of all particles within $R_{\rm vir}$, and the stellar mass was computed as the total mass of stellar particles within $0.1R_{\rm vir}$.

To characterise the inner slope of the dark matter density profile, we computed a linear fit to the logarithmic density profile between 1% and 2% of $R_{\rm vir}$, as in Di Cintio et al. (2014a,b). For this purpose, we adopted the approach from Lazar et al. (2020) to construct dark matter density profiles using 35 logarithmically spaced radial bins between 0.005 $R_{\rm vir}$ and $R_{\rm vir}$. This method was consistently applied to both NIHAO and FIRE-2 galaxies, differing from the binning used for the analysis of NIHAO simulations presented by Tollet et al. (2016).

In Fig. 1, we present the dark matter profile inner slope (measured between 1% and 2% of $R_{\rm vir}$) as a function of the stellar-to-halo mass ratio. We fitted each set of simulations independently using Eq. 2, and we provide the fitted parameters in Table 1. Our results align well with previous findings for and FIRE-2 simulations (Lazar et al. 2020) but notable discrepancies exist between our results for NIHAO simulations and those reported in (Tollet et al. 2016). This mismatch arises from the difference in the definition of virial overdensity used for the analysis, since they adopted the value $\Delta = 200c$[1]. The radius R_{200c} is smaller than $R_{\rm vir}$, and the slope measured by taking it as a reference is inherently more cored than it would by using $R_{\rm vir}$. In Fig. A.1 we show our results when matching this different overdensity definition. Even for FIRE-2 simulations, we note slight discrepancies with the fit from the literature. Some possible origin of these differences could be the algorithm using for centering galaxies or the specific selection of galaxies, as our sample includes more galaxies than previous works for both simulation suites.

After homogenising the analysis across NIHAO and FIRE-2 galaxies, the relation for both simulation suites is in much closer agreement than it could be inferred from previous works, in which the trends derived in Tollet et al. (2016) and Lazar et al. (2020) are compared without taking into account the differences in the analysis. Whilst previous relations indicated that NIHAO galaxies are more efficient at developing shallow dark matter profiles, out results reveal that both simulation suites are capable of forming strong cores. The 1-σ scatter around the relation is also similar: 0.25 for NIHAO and 0.27 for FIRE-2. However, some systematic differences between the two simulation suites remain: whereas we find the peak efficiency of core formation for NIHAO galaxies at $M_\star/M_{\rm vir} \sim 0.005$, FIRE-2 galaxies present their highest count of cored dark matter profiles at $M_\star/M_{\rm vir} \sim 0.008$.

Table 1. Fitted parameters for each set of simulations using Eq. 2 and the overdensity $\Delta = \Delta_{\rm vir}$.

	n	n_1	x_1	x_0	β	γ
NIHAO	-0.87	6.86	8.94×10^{-5}	1.61×10^{-2}	0.78	1.63
FIRE-2	-1.01	3.80	8.54×10^{-4}	2.83×10^{-2}	1.21	1.52

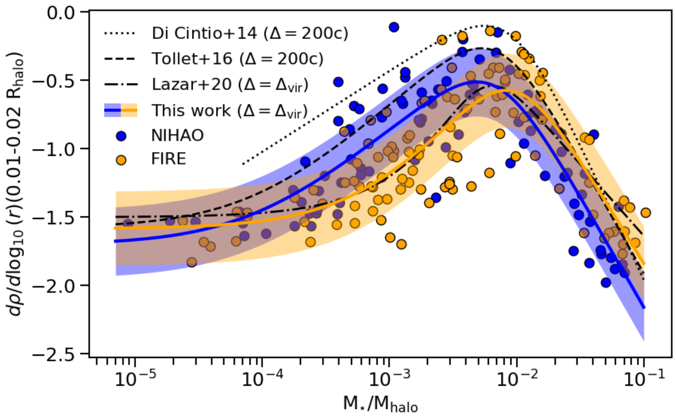

Fig. 1. Inner slope of the dark matter density profile, measured between 1% and 2% of the virial radius, as a function of the stellar-to-halo mass ratio. Results are shown for galaxies from the NIHAO (blue) and FIRE-2 (orange) simulations. Solid lines represent fits following Eq. 2 with parameters from Table 1 and the 1-σ scatter around the fits is indicated with shadowed regions. The trends are compared to literature fits from Di Cintio et al. (2014b), Tollet et al. (2016) and Lazar et al. (2020).

3.1. Burstiness

To quantify burstiness in a galaxy's SFH, we defined a starburst phase using the following criterion:

$$\langle \mathrm{SFR(50\ Myr)} \rangle > 1.5 \, \langle \mathrm{SFR(500\ Myr)} \rangle \tag{3}$$

This is conceptually similar to the approach in Sparre et al. (2017), although we used longer time windows (50 and 500 Myr, compared to their 10 and 200 Myr). Using this definition, we calculated a metric: the *bursty mass fraction*.

Fig. 2 shows how this quantity varies with stellar mass. Compared to the results in Sparre et al. (2017), our criterion produces a more gradually decreasing trend with stellar mass for FIRE-2 galaxies (they did not analyse NIHAO galaxies), which can be well approximated by a second degree polynomial. To characterise individual deviations from this trend, we defined the *burst deviation* as the difference between a galaxy's bursty mass fraction and the value predicted from the polynomial fit at its stellar mass. This deviation quantifies how much more or less bursty a galaxy is than expected for its stellar mass.

[1] Throughout the text, the expression $\Delta = 200c$ denotes an overdensity of 200 times the critical density of the universe, and we use the letter c to explicitly differentiate it from an overdensity of 200 times the average matter density of the universe.

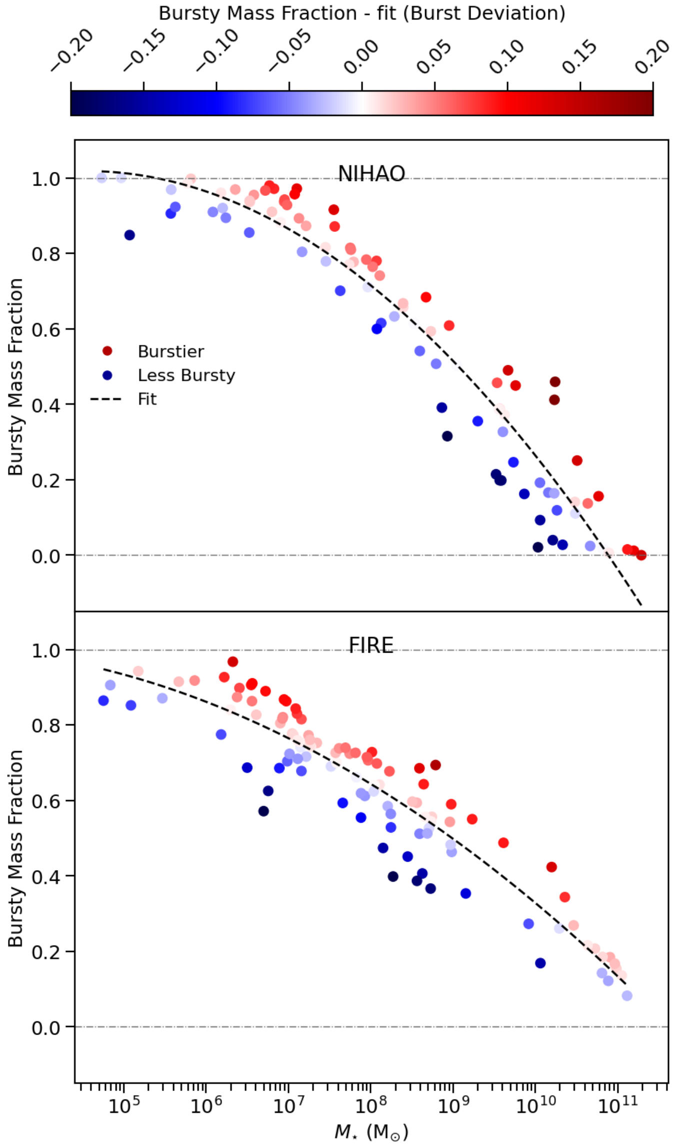

Fig. 2. Bursty mass fractions as a function of stellar mass for galaxies in NIHAO (top panel) and FIRE-2 (bottom panel) simulation suites. Black dashed lines show the result of fitting the bursty mass fraction to the stellar mass with a second degree polynomial. Circles are coloured by their absolute deviation from the fit, which we define as *burst deviation*.

Table 2. Fitted parameters for galaxies with positive and negative burst deviation in each set of simulations using Eq. 2 and the overdensity $\Delta = \Delta_{\rm vir}$.

	NIHAO (>0)	NIHAO (<0)	FIRE-2 (>0)	FIRE-2 (<0)
n	-3.11	-1.33	-0.73	-0.61
n_1	119	1.65	6.52	7.28
x_1	4.71×10^{-9}	1.85×10^{-3}	1.47×10^{-3}	0.93
x_0	1.13	2.63×10^{-2}	1.69×10^{-2}	1.26×10^{-2}
β	0.83	2.27	1.78	348
γ	1.26	1.60	1.52	1.16

In Fig. 3, we plot the inner slope of the dark matter density profile as a function of the stellar-to-halo mass ratio for both NIHAO and FIRE-2 galaxies. This time, each galaxy is coloured by its burst deviation. We fitted separate trends using Eq. 2 for galaxies with positive (more bursty than expected) and negative (less bursty than expected), yielding the parameters in Table 2.

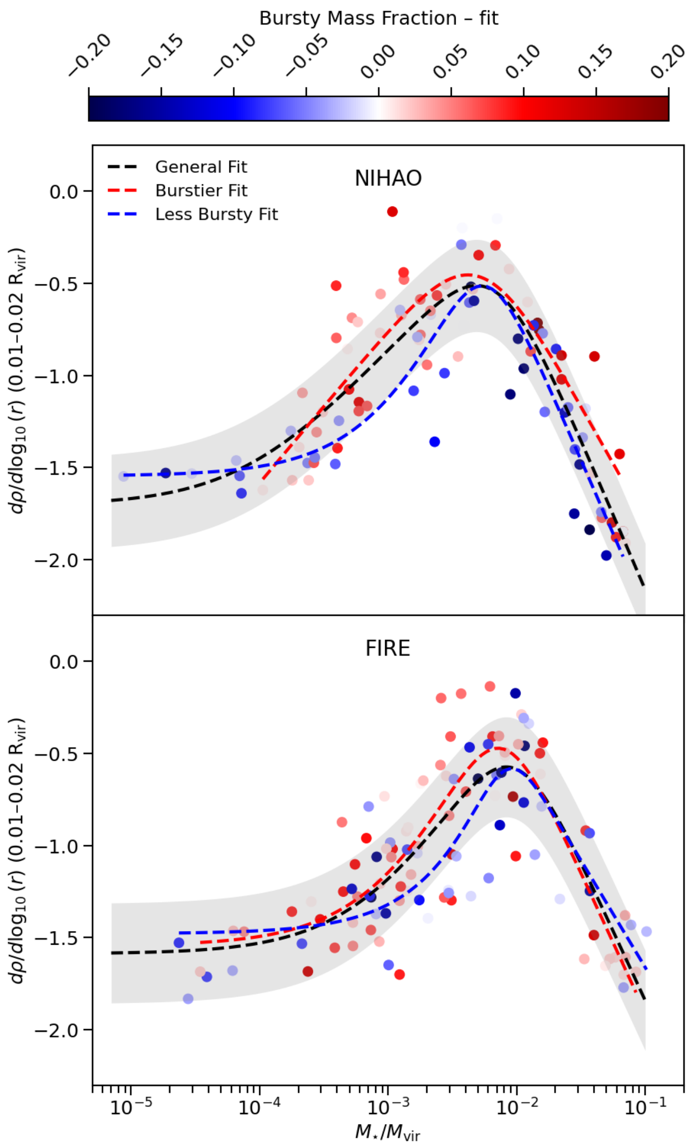

Fig. 3. Inner slope of the dark matter density profile, measured between 1% and 2% of the virial radius, as a function of the stellar-to-halo mass ratio. The top panel shows results for NIHAO galaxies and the bottom panel shows results for FIRE-2 galaxies compared to the literature fit from Lazar et al. (2020). Circles for each galaxy are colour coded by their *burst deviation* (the difference between actual and expected bursty mass fraction at a given stellar mass). Separate fits are shown for galaxies with above- (red dashed lines) and below- (blue dashed lines) average burstiness. Black dashed lines show the fits to the full sample of galaxies from each suite and gray bands represent the 1-σ scatter around the fit. All fits follow Eq. 2 with parameters shown in Table 2.

For NIHAO galaxies, the trend is clear: galaxies that are burstier than the average for their stellar mass are more likely to exhibit cored dark matter profiles. The trend is similar in the FIRE-2 sample for mass ratios at and just below the peak in core formation ($M_\star/M_{\rm vir} \sim 0.005$-$0.008$) but disappears for $M_\star/M_{\rm vir} > 0.02$, where we find a gap in the galaxies from the sample.

3.2. SFH duration

In addition to burstiness, we explored how the temporal distribution of star formation (specifically, its duration relative to the epoch of reionisation) affects the inner dark matter slope. To this end, we defined two quantities:

$$M_{\star,\mathrm{pre}} = \int_{t=0}^{t_{\mathrm{reion}}} \mathrm{SFR}dt \quad (4)$$

$$M_{\star,\mathrm{post}} = \int_{t=t_{\mathrm{reion}}}^{t_{\mathrm{today}}} \mathrm{SFR}dt \quad (5)$$

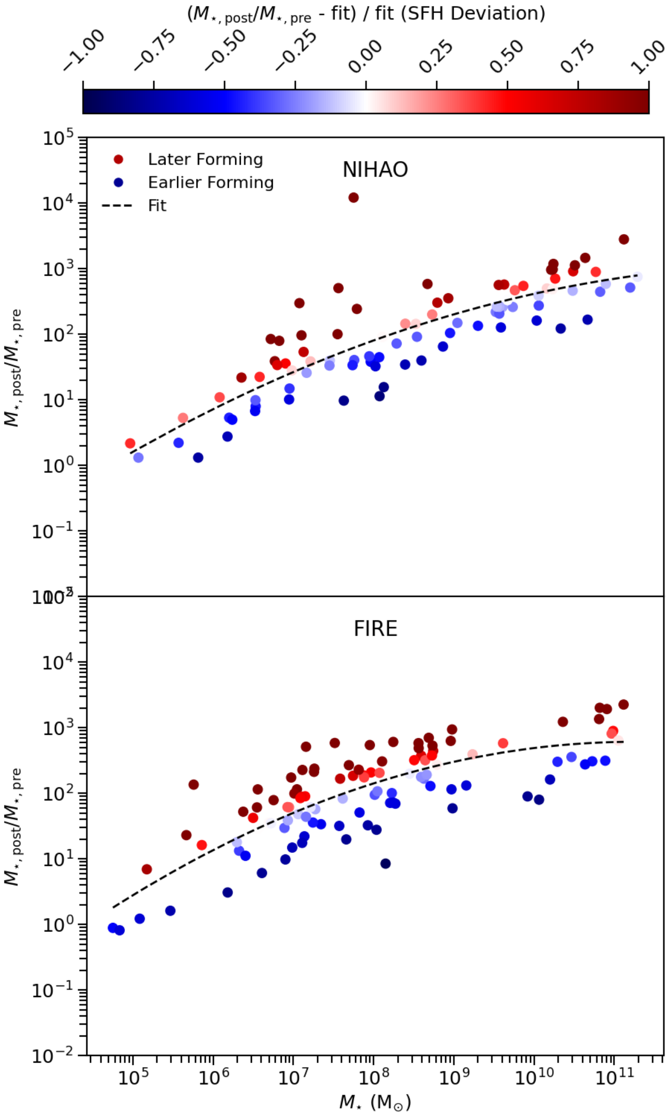

Fig. 4. Ratio of post- to pre-reionisation stellar mass ($M_{\star,\mathrm{post}}/M_{\star,\mathrm{pre}}$) as a function of total stellar mass for galaxies in NIHAO (top panel) and FIRE-2 (bottom panel) simulation suites. Black dashed lines show second degree polynomial fits. Circles are coloured by their relative deviation from the fit, which we define as *SFH deviation*.

These follow the definitions in Muni et al. (2024), using $z_{\mathrm{reion}} = 6.5$ ($t_{\mathrm{reion}} = 0.84$ Gyr) motivated by the Faucher-Giguère et al. (2009) ultraviolet background model that controls the reionisation process in both EDGE and FIRE-2 simulations. Although

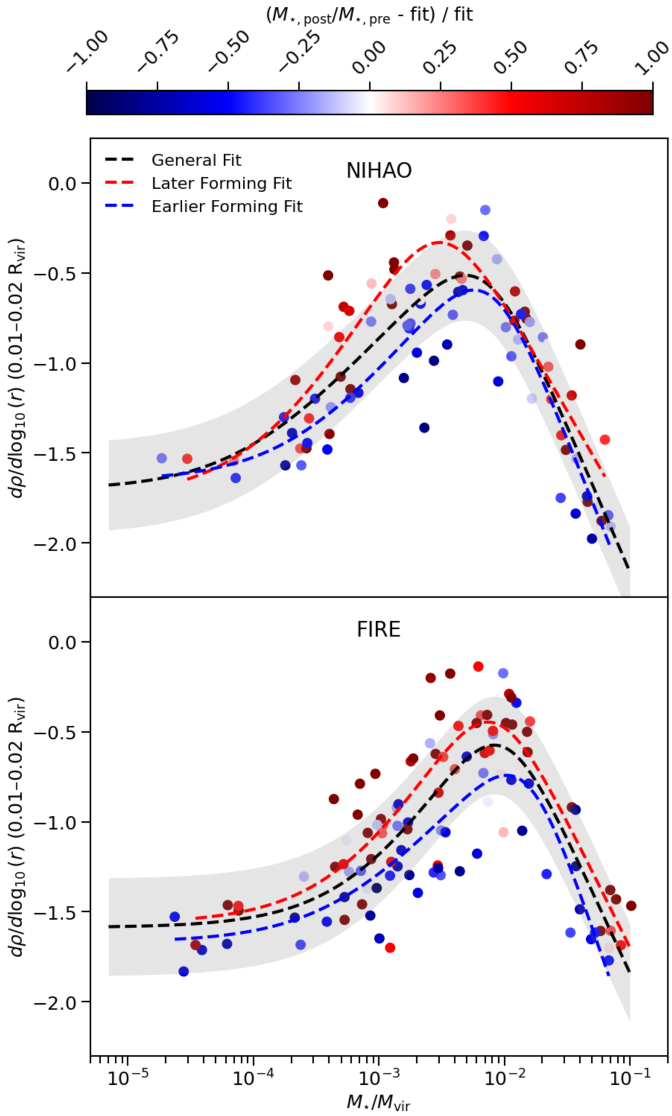

Fig. 5. Inner slope of the dark matter density profile, measured between 1% and 2% of the virial radius, as a function of the stellar-to-halo mass ratio. The top panel shows results for NIHAO galaxies and the bottom panel shows results for FIRE-2 galaxies. Circles for each galaxy are colour coded by their *SFH deviation* (the relative difference between actual and expected post- to pre-reionisation stellar mass ratio at a given stellar mass). Separate fits are shown for galaxies with more extended (red dashed lines) and less extended (blue dashed lines) SFHs. Black dashed lines show the fits to the full sample of galaxies from each suite and gray bands represent the 1-σ scatter around the fit. All fits follow Eq. 2 with parameters shown in Table 3.

NIHAO galaxies use a different model, the time scale in which reionisation occurs is comparable.

The ratio $M_{\star,\mathrm{post}}$ / $M_{\star,\mathrm{pre}}$ serves as a proxy for the temporal extent of the SFH[2]. We observe that this ratio increases with stellar mass, as illustrated in Fig. 4. As expected, more massive galaxies are more efficient at converting baryons into stars, tending to form stars over more extended periods of time. Note that both the NIHAO and FIRE-2 galaxies in our sample are isolated,

[2] A small subsample of galaxies lack any star formation before z = 6.5, resulting in intractable $M_{\star,\mathrm{post}}$ / $M_{\star,\mathrm{pre}}$ values. We remove them for the analyses that include this feature, resulting in 90 NIHAO and 108 FIRE-2 galaxies.

and not subject to quenching due to environmental factors. To quantify individual deviations from this trend, we defined the *SFH deviation* as the fractional difference between a galaxy's $M_{\star,\mathrm{post}}$ / $M_{\star,\mathrm{pre}}$ ratio and the value predicted by a second degree polynomial fit to the stellar mass.

Using the *SFH deviation*, we classified galaxies into two groups and analysed their corresponding trends in inner dark matter slope versus stellar-to-halo mass ratio, as shown in Fig. 5. Resulting parameters from the fits to Eq. 2 can be found in Table 3. The results reveal that galaxies with more extended SFHs (higher than expected $M_{\star,\mathrm{post}}$ / $M_{\star,\mathrm{pre}}$) tend to have shallower inner dark matter profiles compared to galaxies with more concentrated SFHs. This pattern holds for both the NIHAO and FIRE-2 simulation suites.

Table 3. Fitted parameters for galaxies with positive and negative SFH deviation in each set of simulations using Eq. 2 and the overdensity $\Delta = \Delta_{\mathrm{vir}}$.

	NIHAO (>0)	NIHAO (<0)	FIRE-2 (>0)	FIRE-2 (<0)
n	-1.00	-0.83	-0.92	-0.99
n_1	5.73	6.63	4.37	4.73
x_1	1.34×10^{-4}	2.44×10^{-4}	6.43×10^{-4}	4.88×10^{-4}
x_0	1.90×10^{-2}	1.48×10^{-2}	2.84×10^{-2}	2.61×10^{-2}
β	1.26	0.89	1.26	0.79
γ	1.21	1.76	1.42	2.06

Muni et al. (2024) performed additional analyses of how the $M_{\star,\mathrm{post}}$ / $M_{\star,\mathrm{pre}}$ ratio influences dark matter profile shapes, employing alternative coreness indicators rather than the 1–2% R_{vir} slope used in this work. We reproduce their tests and present the corresponding results in Appendix B.

3.3. Second order correction to the inner slope fit

We have demonstrated that both burstiness and the duration of the SFH play a role, separate from the star-to-halo mass ratio, in shaping the inner region of the dark matter density profile of halos. We now aim to use these features to obtain a correction term over the fitting by Eq. 2. We decided to use only one of the features at a time, since we find them to be correlated, as we show in Fig. 6. In that figure we also notice an outlier galaxy with a very high $M_{\star,\mathrm{post}}$ / $M_{\star,\mathrm{pre}}$ value, which can also be observed in Fig. 4. While this galaxy does not introduce any notable effect in the previous analysis, we decide to remove it for the fitting performed in this section.

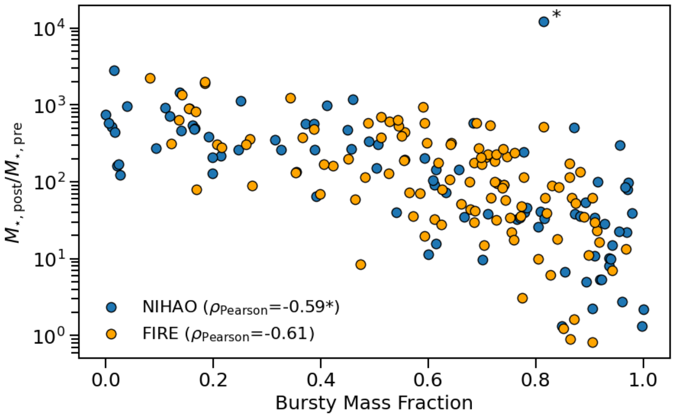

Fig. 6. Relation between $M_{\star,\mathrm{post}}$ / $M_{\star,\mathrm{pre}}$ and the bursty mass fraction for NIHAO and FIRE-2 galaxies. The Pearson correlation coefficient is indicated in the legend. One outlier NIHAO galaxy, marked with an asterisk, is removed from the calculation.

We report a two variable fitting formula for the inner slope described by Eq. 6, where x = $M_\star/M_{\mathrm{vir}}$ and y = $M_{\star,\mathrm{post}}$ / $M_{\star,\mathrm{pre}}$. The inclusion of the additional correction lowers the mean squared error in the prediction of the inner slope from 0.073 to 0.055 for FIRE-2 galaxies, and from 0.063 to 0.048 for NIHAO galaxies. We show the fitted parameters for each simulation suite in Table 4. In Fig. 7 we visualise the fit by plotting the trend of the inner slope with the stellar-to-halo mass ratio for different values of $M_{\star,\mathrm{post}}$ / $M_{\star,\mathrm{pre}}$. In the figure we can observe how, for the same ratio of stellar mass to halo mass, galaxies are more likely to present shallower density profiles when they have undergone extended SFHs (high values of $M_{\star,\mathrm{post}}$ / $M_{\star,\mathrm{pre}}$).

$$\left.\frac{d\rho}{d\log_{10} r}\right|_{r=0.015R_{\mathrm{halo}}}(x) = n - \log_{10}\left[n_1\left(1+\frac{x}{x_1}\right)^{-\beta} + \left(\frac{x}{x_0}\right)^{\gamma}\right] + n_2 y^{\alpha} \tag{6}$$

Table 4. Fitted parameters for each set of simulations using Eq. 6 and the overdensity $\Delta = \Delta_{\mathrm{vir}}$.

	n	n_1	n_2	x_1	x_0	β	γ	α
NIHAO	-84.5	84.2	32.1	2.73×10^{-4}	2.87×10^{-3}	0.67	1.75	1.35×10^{-3}
FIRE-2	-2.34	0.51	0.83	3.17×10^{-3}	3.31×10^{-2}	1.45	1.75	0.14

4. Conclusions

In this work, we revisited the dependence of the inner slope of dark matter density profiles on the stellar-to-halo mass ratio using homogeneously analysed samples from the NIHAO and FIRE-2 simulations. Our results bring the two suites into closer agreement, showing that careful methodological consistency is essential when comparing simulations and interpreting apparent differences across studies. Whereas earlier comparisons between the analyses of Tollet et al. (2016) and Lazar et al. (2020) suggested that NIHAO galaxies were intrinsically more prone to developing cored dark matter profiles than those in FIRE-2, our homogeneous reanalysis shows that both simulation suites are capable of producing galaxies with similarly cored inner density structures. However, the stellar-to-halo mass ratio at which core formation is most efficient is slightly lower for NIHAO galaxies than for the FIRE-2 suite.

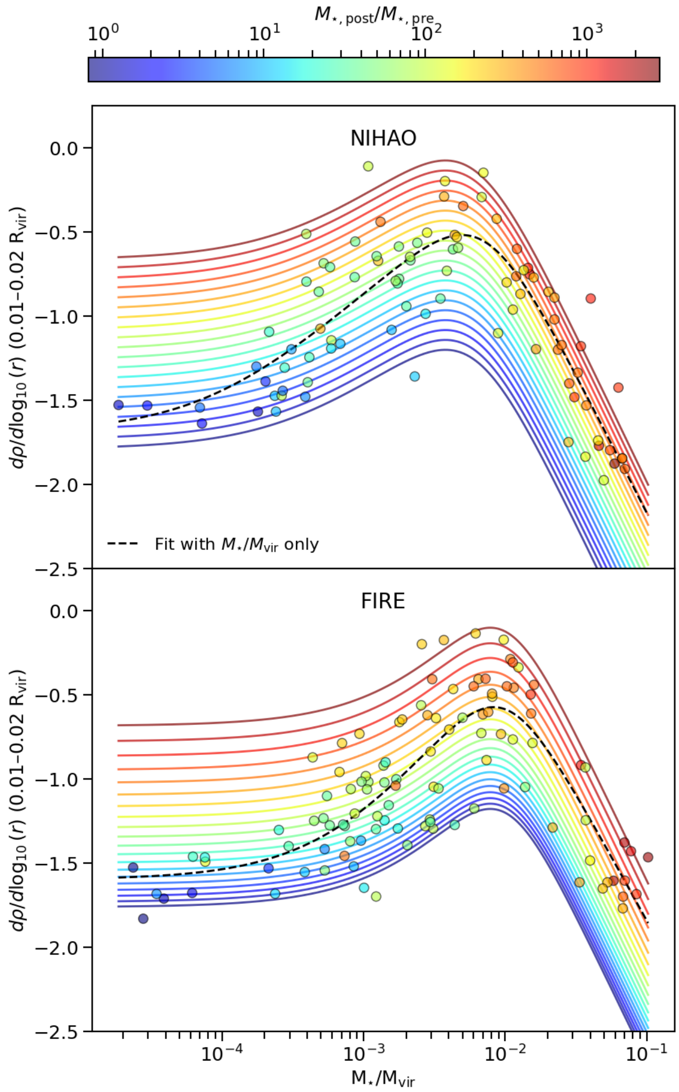

Fig. 7. True values (circles) and predictions (lines) for the inner slope of the dark matter density profile as a function of the stellar-to-halo mass ratio for different values of $M_{\star,\mathrm{post}}$ / $M_{\star,\mathrm{pre}}$ via the fit by Eq. 6 with the parameters shown in Table 4. Black dashed lines indicate fits using only the stellar-to-halo mass ratio, described by the parameters in Table 1 for Eq. 2. The top panel shows the results for the NIHAO suite and the bottom panel corresponds to the galaxies from the FIRE-2 dataset.

We quantified star formation burstiness by adapting the burst criterion introduced in Sparre et al. (2017), deriving burst mass fractions that trace how concentrated in time star formation is within a galaxy. We find that burstiness decreases systematically with increasing stellar mass in the range $M_\star \sim 10^5 - 10^{11}$ $M_\odot$.

To characterise the temporal duration of SFHs, we employed the $M_{\star,\mathrm{post}}/M_{\star,\mathrm{pre}}$ ratio introduced by Muni et al. (2024). In both NIHAO and FIRE-2 galaxies, higher stellar mass systems exhibit more extended SFHs.

By fitting the dependence of burstiness and SFH duration on stellar mass, we identified residuals that highlight galaxies which are more or less bursty, or have longer or shorter SFHs, than the average for their mass. These deviations act as secondary predictors of dark matter core formation, beyond the primary role of the stellar-to-halo mass ratio. Specifically, we find that galaxies which are burstier than average develop shallower inner dark matter slopes. Similarly, those with more extended SFHs are more efficient at producing cores. These SFH features explain the existing scatter in the relation between the inner slope and the stellar-to-halo mass ratio in both simulation suites.

We also derived a new fitting formula for the inner slope that includes the contribution of the SFH duration via the $M_{\star,\mathrm{post}}/M_{\star,\mathrm{pre}}$ ratio (Eq. 6). The addition of a simple term and the joint fitting to data from each simulation revealed higher accuracy than using only the stellar-to-halo mass ratio as a fitting variable, lowering the mean squared error from 0.073 to 0.055 for FIRE-2 galaxies and from 0.063 to 0.048 for NIHAO simulations.

Our analysis suggests that burstiness and SFH duration capture important aspects of the baryonic processes that shape dark matter profiles. However additional factors, such as the relative strength and timing of starbursts or their spatial distribution within galaxies, are likely to play a significant role. Exploring these features will be the focus of future work.

The predicted relationship between core formation and SFH at fixed stellar mass has significant observational implications. Advances in resolved stellar population studies now enable accurate SFH measurements for low mass galaxies well beyond the virial radius of the Milky Way (e.g. Weisz et al. 2023; Cohen et al. 2025). We predict that galaxies with stellar masses of $M_\star \sim 10^8 M_\odot$, situated near the peak of core formation efficiency ($M_\star/M_{\mathrm{vir}} \sim 0.005$), should display structural differences driven by their assembly age. Specifically, systems with stellar age distributions biased towards early times are expected to retain cuspier profiles than similar mass galaxies with extended, late time star formation. Observing large cores in objects dominated by early star formation would contradict this prediction, suggesting that feedback mechanisms alone are insufficient and pointing toward alternative scenarios such as Self-Interacting Dark Matter (SIDM).

Acknowledgements. JSA thanks the Spanish Ministry of Economy and Competitiveness (MINECO) for support through a grant P/301404 from the Severo Ochoa project CEX2019-000920-S and the Fostering Grads organisation for sponsoring the ECUSA program, which made this international collaboration possible. JSB is supported by NSF grant AST-2408246. CB is supported by the Spanish Ministry of Science and Innovation (MICIU/FEDER) through research grant PID2021-122603NBC22. ADC is supported by the Agencia Estatal de Investigación, under the 2023 call for Ayudas para Incentivar la Consolidación Investigadora, grant number CNS2023-144669, project "TINY". The authors wish to acknowledge the contribution of the IAC High-Performance Computing support team and hardware facilities to the results of this research. The freely available software pynbody (Pontzen et al. 2013) has been used for part of this analysis. We thank the PI of the FIRE-2 simulation projects for making their data publicly available at http://flathub.flatironinstitute.org/fire.

References

Agertz, O., Pontzen, A., Read, J. I., et al. 2019, MNRAS, 491, 1656
Brook, C. B. & Di Cintio, A. 2015, MNRAS, 453, 2133
Brook, C. B., Stinson, G., Gibson, B. K., Wadsley, J., & Quinn, T. 2012, MNRAS, 424, 1275
Bryan, G. L. & Norman, M. L. 1998, ApJ, 495, 80
Chabrier, G. 2003, PASP, 115, 763
Cohen, R. E., McQuinn, K. B. W., Savino, A., et al. 2025, ApJ, 981, 153
de Blok, W. J. G., McGaugh, S. S., & Rubin, V. C. 2001, AJ, 122, 2396
Di Cintio, A., Brook, C. B., Dutton, A. A., et al. 2017, MNRAS, 466, L1
Di Cintio, A., Brook, C. B., Dutton, A. A., et al. 2014a, MNRAS, 441, 2986
Di Cintio, A., Brook, C. B., Macciò, A. V., et al. 2014b, MNRAS, 437, 415
Emami, N., Siana, B., Weisz, D. R., et al. 2019, ApJ, 881, 71
Faucher-Giguère, C.-A., Lidz, A., Zaldarriaga, M., & Hernquist, L. 2009, ApJ, 703, 1416
Graus, A. S., Bullock, J. S., Fitts, A., et al. 2019, MNRAS, 490, 1186
Haardt, F. & Madau, P. 2012, ApJ, 746, 125
Hopkins, P. F. 2015, MNRAS, 450, 53

Hopkins, P. F., Wetzel, A., Kereš, D., et al. 2018, MNRAS, 480, 800–863
Kim, J.-h., Abel, T., Agertz, O., et al. 2014, ApJS, 210, 14
Knollmann, S. R. & Knebe, A. 2009, ApJS, 182, 608
Lazar, A., Bullock, J. S., Boylan-Kolchin, M., et al. 2020, MNRAS, 497, 2393
Macciò, A. V., Stinson, G., Brook, C. B., et al. 2012, ApJ, 744, L9
Muni, C., Pontzen, A., Read, J. I., et al. 2024, MNRAS, 536, 314–323
Navarro, J. F., Eke, V. R., & Frenk, C. S. 1996, MNRAS, 283, L72–L78
Navarro, J. F., Frenk, C. S., & White, S. D. M. 1997, ApJ, 490, 493
Oh, S.-H., de Blok, W. J. G., Brinks, E., Walter, F., & Kennicutt, R. C. 2011, ApJ, 141, 193
Peñarrubia, J., Pontzen, A., Walker, M. G., & Koposov, S. E. 2012, ApJ, 759, L42
Planck Collaboration, Ade, P. A. R., Aghanim, N., et al. 2014, A&A, 571, A16
Pontzen, A. & Governato, F. 2012, MNRAS, 421, 3464
Pontzen, A. & Governato, F. 2014, Nature, 506, 171–178
Pontzen, A., Roškar, R., Stinson, G. S., et al. 2013, pynbody: Astrophysics Simulation Analysis for Python, astrophysics Source Code Library, ascl:1305.002
Read, J. I., Agertz, O., & Collins, M. L. M. 2016, MNRAS, 459, 2573
Read, J. I. & Gilmore, G. 2005, MNRAS, 356, 107
Rey, M. P., Taylor, E., Gray, E. I., et al. 2025, EDGE: The emergence of dwarf galaxy scaling relations from cosmological radiation-hydrodynamics simulations
Shen, S., Wadsley, J., & Stinson, G. 2010, MNRAS, 407, 1581–1596
Sparre, M., Hayward, C. C., Feldmann, R., et al. 2017, MNRAS, 466, 88
Stinson, G., Seth, A., Katz, N., et al. 2006, MNRAS, 373, 1074
Stinson, G. S., Brook, C., Macciò, A. V., et al. 2013, MNRAS, 428, 129
Tollet, E., Macciò, A. V., Dutton, A. A., et al. 2016, MNRAS, 456, 3542
Wadsley, J. W., Keller, B. W., & Quinn, T. R. 2017, Monthly Notices of the Royal Astronomical Society, 471, 2357
Wang, L., Dutton, A. A., Stinson, G. S., et al. 2015, Monthly Notices of the Royal Astronomical Society, 454, 83
Weisz, D. R., Johnson, B. D., Johnson, L. C., et al. 2012, ApJ, 744, 44
Weisz, D. R., McQuinn, K. B. W., Savino, A., et al. 2023, ApJS, 268, 15

Appendix A: Analysing the inner slope with $\Delta = 200c$

For this work, we adopted the virial overdensity Δ_{vir} defined in Bryan & Norman (1998) to analyse the FIRE-2 and NIHAO simulations homogeneously. Nonetheless, several studies (e.g. Di Cintio et al. 2014b; Tollet et al. 2016) use a fixed overdensity of $\Delta = 200c$ to investigate the relation between the inner slope of the dark matter density profile and the stellar-to-halo mass ratio. To facilitate a direct comparison to these works, we repeat our analysis using $\Delta = 200c$. For this purpose, we construct new density profiles analogous to those presented in Fig. 2 of Tollet et al. (2016), employing 56 logarithmically spaced bins spanning the range 0.01–1 R_{200c}.

We again apply Eq. 2 to fit the inner slope of the dark matter density profile, measured between 1–2% R_{200c}, as a function of the stellar-to-halo mass ratio $M_\star/M_{200c}$ (see fitted parameters in Table A.1). The resulting relation is shown in Fig. A.1. Using the overdensity definition adopted by Tollet et al. (2016) produces a relation more consistent with their results, and galaxies with shallower profiles display even flatter inner slopes due to the more internal measurement radius. The scatter in the relation also increases, reaching 0.27 for NIHAO and 0.29 for FIRE-2. In addition, the stellar-to-halo mass ratio at which the profiles are maximally shallow shifts to higher values: 0.005 for NIHAO and 0.009 for FIRE-2. We note that the NIHAO peak value has increased slightly relative to our previous analysis, even though it rounds to the same value at one significant digit.

Table A.1. Fitted parameters for each set of simulations using Eq. 2 and the overdensity $\Delta = 200c$.

	n	n_1	x_1	x_0	β	γ
NIHAO	-1.09	4.31	3.24×10^{-5}	2.63×10^{-2}	0.70	1.88
FIRE-2	-0.85	4.86	4.43×10^{-4}	2.90×10^{-2}	0.98	1.70

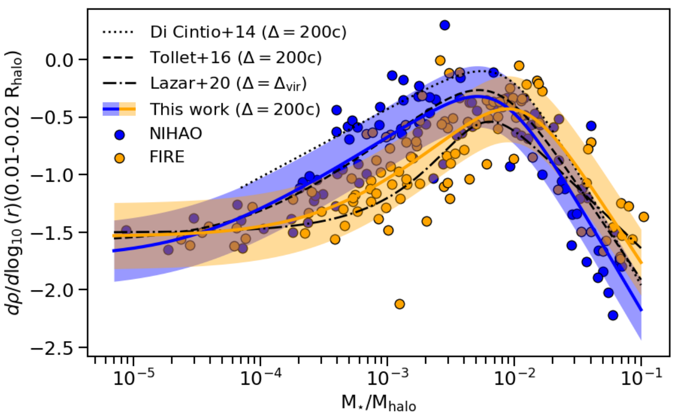

Fig. A.1. Inner slope of the dark matter density profile, measured between 1% and 2% of R_{200c}, as a function of the stellar-to-halo mass ratio. Results are shown for galaxies from the NIHAO (blue) and FIRE-2 (orange) simulations. Solid lines represent fits following Eq. 2 and the 1-σ scatter around the fits is indicated with shadowed regions. The trends are compared to literature fits from Di Cintio et al. (2014b), Tollet et al. (2016) and Lazar et al. (2020).

Appendix B: Comparing results between EDGE and FIRE-2

Muni et al. (2024) analysed core formation in EDGE1 and EDGE2 simulations (Agertz et al. 2019; Rey et al. 2025) by measuring the dark matter density at 150 pc from galaxy centers. They reported a tight, decreasing linear relation between the inner dark matter density and the ratio $M_{\star,\mathrm{post}}/M_{\star,\mathrm{pre}}$. We replicate this analysis using FIRE-2 galaxies to calculate their density within a spherical shell ranging from 125 to 175 pc, with results shown in Fig. B.1. NIHAO galaxies are excluded due to insufficient spatial resolution. For some FIRE-2 galaxies, the 150 pc region lies within the r_{200}[3] resolution limit; however, we check that extrapolating the resolved density profile confirms that the inner densities do not significantly deviate from expected values. Additionally, we plot the density at the innermost resolved bin, providing a lower limit for the density at 150 pc.

Within the range of $M_{\star,\mathrm{post}}/M_{\star,\mathrm{pre}}$ values probed by EDGE simulations, we also recover a decreasing linear relation between inner density and $M_{\star,\mathrm{post}}/M_{\star,\mathrm{pre}}$. The trend is steeper for FIRE-2 galaxies, which also exhibit higher scatter. At higher $M_{\star,\mathrm{post}}/M_{\star,\mathrm{pre}}$ ratios, however, FIRE-2 galaxies show increased inner densities. We attribute this trend change to the broader stellar mass range in our sample. The relation for FIRE-2 galaxies is fitted using Eq. B.1 with $x = M_{\star,\mathrm{post}}/M_{\star,\mathrm{pre}}$. The resulting fitted parameters are: $x_0 = 2.14\times10^3, n = -6.22\times10^{-2}, \beta = 8.12\times10^{-2}$ and $\gamma = 1.98$. The resulting fitted relation is qualitatively similar to the classical relation between the dark matter density inner slope and the stellar-to-halo mass ratio (see e.g. Fig. 1 and Eq. 1).

$$\frac{\rho_{150\mathrm{pc}}(x)}{10^9 M_\odot kpc^{-3}} = n + \log_{10}\left[\left(\frac{x}{x_0}\right)^{-\beta} + \left(\frac{x}{x_0}\right)^{\gamma}\right] \quad \text{(B.1)}$$

Muni et al. (2024) also report a tight correlation between the $M_{\star,\mathrm{post}}$ / $M_{\star,\mathrm{pre}}$ and the inner slope of the dark matter density profile. They illustrate the dependency using the n variable of the coreNFW profile introduced by Read et al. (2016). In Fig. B.2 we compare their findings with the results of fitting the same profile to our dataset of FIRE-2 galaxies. Following their methodology, we fixed the core radius parameter (r_c) of the coreNFW profile to 1.8 times the three dimensional V-band half-light radius of the galaxy to break the degeneracy with the n parameter when fitting the dark matter density profile. Additionally, we fix the halo mass to the value derived from the simulation and constrain n to lie between 0 and 1. We note that the fixed core radius does not provide satisfactory fits for some galaxies in our sample, which span a broader range of stellar and halo properties than the EDGE simulations. Nevertheless, we confirm via visual inspection that the inner slope of the fitted profile generally matches the data. To quantify the fit quality, we compute the median relative deviation of the model from the data, finding that values above ~ 0.15 typically indicate unreliable fits near the core radius. Overall, we find that, due to these fitting limitations, the n parameter is less reliable as a tracer of galactic coreness than the directly measured inner slope of the density profile. We notice FIRE-2 galaxies exhibit lower n values (cuspier) than EDGE galaxies for the same $M_{\star,\mathrm{post}}$ / $M_{\star,\mathrm{pre}}$, indicating they require more extended SFHs for developing equally shallow density profiles. On top of that, the relation between n and the post- and pre-reionisation stellar mass ratio is much more disperse for FIRE-2 galaxies, which do not follow a clear trend.

[3] The radius that encloses 200 dark matter particles.

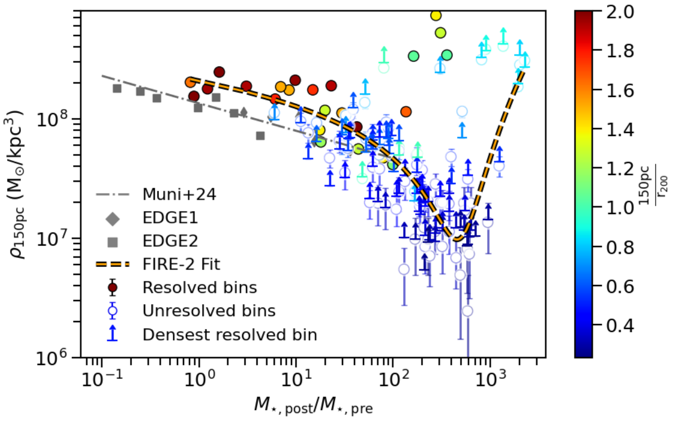

Fig. B.1. Dark matter density at 150 pc versus the ratio of stellar mass formed after and before reionisation. Gray symbols indicate Muni et al. (2024) results for EDGE galaxies, and the dash-dotted line shows their linear fit. Filled (empty) circles indicate the inner densities of FIRE-2 galaxies that are (un)resolved at 150 pc, with errorbars representing poisson uncertainties associated to the number of dark matter particles used to calculate the inner density. Markers are colored based on the ratio between 150 pc and the power radius r_{200}, which marks the resolution limit. For unresolved points, horizontal lines provide a lower limit to the inner density by taking the densest resolved bin in the density profile. The orange dashed line represents the fit to the inner densities, including unresolved bins.

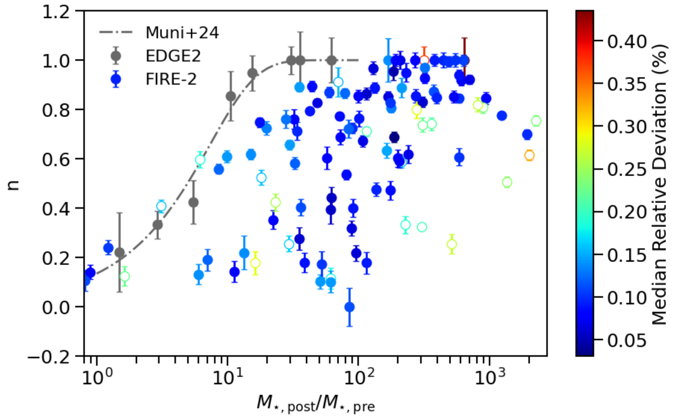

Fig. B.2. n parameter of the coreNFW profile versus the ratio of stellar mass formed after and before reionisation. Gray circles with errorbars show the results for EDGE2 galaxies and coloured plots indicate the fitted values for galaxies from the FIRE-2 suite. Colours indicate the fit quality via the median deviation of the model relative to the data. Galaxies with median relative deviation over 0.15% are displayed as empty circles, indicating unreliable fitting around the core radius. The gray dot-dashed line represents the fit to the EDGE2 simulations reported by Muni et al. (2024).